2022

CFD Study of the Internal Leakage of a Four-Intersecting-Vane Expander

Anarghya Ananda Murthy

Alison Subiantoro

CFD Study of the Internal Leakages of a Four-Intersecting-Vane Expander in Static Conditions

Anarghya Ananda MURTHY[1]*, Alison SUBIANTORO[1]

[1]The University of Auckland, Department of Mechanical and Mechatronics Engineering, Auckland, New Zealand
E-mail: amur812@aucklanduni.ac.nz

* Corresponding Author

ABSTRACT

Leakage has a strong negative impact on the performance of a positive displacement machine. In this work, the internal leakages of a four-intersecting-vane expander is investigated using a computational fluid dynamics (CFD) approach. The mechanism is similar to typical rotary vane machines, but the vanes are made up of intersecting bars and the inner wall of the stator is not circular. A 3D steady state CFD simulation model was developed in ANSYS FLUENT. The geometry was based on a prototype that was previously experimented on by the authors. The model was used to simulate the leakage flows along the main internal leakage paths using compressed air as the working fluid. These include the gaps between: 1) the rotor outer wall and the stator inner wall at its nearest section, called the radial clearance, 2) the vane tips and the stator inner wall, called the vane tip gaps, and 3) the end faces of the stator and those of the rotor and the vanes. The other leakage gaps were ignored because previous experiments had shown that they were less important. The suction pressure was varied from 0.5 bar(g) to 5 bar(g), while the discharge pressure was constant at 0 bar(g). The study investigates in detail the leakage flow rates, pressure distributions and Mach numbers, which are difficult to analyze in an experiment. Validation of the model shows that the simulation results showed similar trends with previously published experimental data. However, discrepancies were observed with the values because of the constant gaps assumption in the simulation. In conclusion, the study shows that CFD can study the internal leakages of a four-intersecting-vane expander but more realistic settings are needed to generate more accurate predictions.

1. INTRODUCTION

Improving the performance of compressor and expander machines has been one of the drivers for both academic research and industrial development for many decades (Thakur et al., 2019). Out of all the available mechanisms, the rotary vane machine is among the oldest. The invention of this mechanism can be dated back to 1874, by Charles C Barnes in Canada, whereas rotary vane compressors, comprising a stator, a rotor, and vanes originated in 1967 (Bellmer, 1967). The rotary vane mechanism has a higher power density, lower vibration, and lower parts than conventional piston engines (Mathieu et al., 2016a; 2016b). Rotary vane machines are used as pumps in automotive (Wang et al., 2012; Cipollone et al., 2015), compressed air systems (Vittorini et al., 2016), oil and gas fields (Tang et al., 2016) and, more recently, as expanders for CO_2 refrigeration system (Fukuta et al., 2003; Murthy et al., 2019), for non-CO_2 refrigeration system (Murthy et al., 2021a) and Organic Rankine Cycle (ORC) (Cipollone et al., 2014), and even for non-conventional applications such as atmospheric freeze drying (Liu et al., 2021)

These machines are commonly studied using experimental methods (Bianchi et al., 2015a; Huang et al., 2005), or a theoretical approach, conventionally with a lumped parameter formulation of the conservation equations with homogeneous spatial variation of values (Badr et al., 1985; Tramschek et al., 1996; Al-Hawag, 2009; Bianchi et al., 2015b). With the advancement of CFD techniques, it is now possible to apply the equations governing fluid motions to a wide range of complex situations, resulting in both insights and quantitative predictions. Some commercial software companies (such as Simerics, ANSYS) have made the Computational Fluid Dynamics (CFD) solver more popular. To this end, the lack of general, parametric and effective techniques to discretize the working chamber volumes is the fundamental constraint for using state-of-the-art design tools like Computational Fluid Dynamics

(CFD) software. Particularly, for a rotary vane expander, this volume is formed by a stator, several vanes/blades and a rotor. This research gap has started to be addressed with some recent CFD works on the machine. Montenegro et al. (2014) developed a CFD model for a rotary vane expander with elliptic stator. Kolasiński and Błasiak, (2016) performed numerical and experimental studies on a rotary vane expander with circular stator for an ORC system. Some works have been reported on the development of a dynamic CFD model for rotary vane expander (Bianchi et al., 2017). Meanwhile, a typical rotary vane expander has main four leakage paths: (a) The clearance between the vane slot and the vane, (b) The clearance between the end surfaces of the stator and the rotor, (c) The radial clearance between the stator's inner wall and the rotor's outer wall, and (d) The clearance between the tip of the vanes and the stator inner wall (Yang et al., 2009). CFD is useful to study the internal leakages of a rotary vane expander, but most of the rotary vane expander numerical studies in the literature were performed by focusing on the leakage at the vane tip gap because it is challenging to employ precise representation of all the leakage paths, particularly when the mesh is allowed to deform and with a moving computational domain (Bianchi et al., 2017). Meanwhile, the experimental studies of expanders usually only provide the macro-scale phenomena, such as the power output, flow rate, pressure and temperature. However, some microscopic problems, such as the internal leakages are very difficult to be detected with the experimental techniques, particularly in a dynamic setting. CFD offers a way to examine the flow structure inside an expander and investigate crucial aspects such as expansion process and internal leakages, all of which affect the expander's efficiency.

In this paper, the authors' attempt to investigate the internal leakages of a rotary expander with four vanes in static conditions using CFD method is presented. The mechanism is different from a conventional rotary vane machine and is called the four-intersecting-vane mechanism. The vanes are formed by two intersecting long bars, instead of four separate vanes. To maintain contact between the vanes and the stator, the inner wall of the stator has a varying diameter, while the distance between two points on the stator inner wall passing the centre of the rotor is always constant to allow the bars to rotate properly. More detailed description of the mechanism can be found in the authors' previous works (Murthy et al., 2021a, 2021b, 2022b). In the current work, the expander's CFD model is developed by including the leakages at the radial, vane tip and rotor-vane endface clearances. The other leakages paths are ignored as they have been shown to be less important previously and the results obtained are then compared against the experimental data in the literature (Murthy et al., 2022a).

2. MODELLING OF FOUR-INTERSECTING-VANE EXPANDER AND GRID DETAILS

A four-intersecting-vane rotary expander is a positive displacement device consisting of a rotating cylinder called rotor inside a fixed cylinder named stator. The rotor rotates inside the stator and contains four slots in which blades called vanes partition the interior into working chambers. The vanes are made of two intersecting long bars. The stator inner wall is not circular, instead its profile is such that the vanes can move properly while maintaining contacts at the tips. The line contact between the stator and the rotor is defined as the 0° point. The center of the suction port is located 10° angle away from this line contact. The discharge port is shaped like a groove extending from an angle of 225° to 340°. Figure 1 shows the modelled geometry of the four-intersecting-vane expander.

The main dimensions of the expander are listed in Table 1. It is useful to note that the clearance gap sizes were obtained from measurements of the expander when it was disassembled. The actual sizes after assembly and during operation were not known, and could differ from the values listed in the table. ANSYS FLUENT 2019 R2 was used to perform analyses with air as the working fluid, modelled as an ideal gas under adiabatic conditions. The model settings and boundary conditions applied on the zones are tabulated in Table 2.

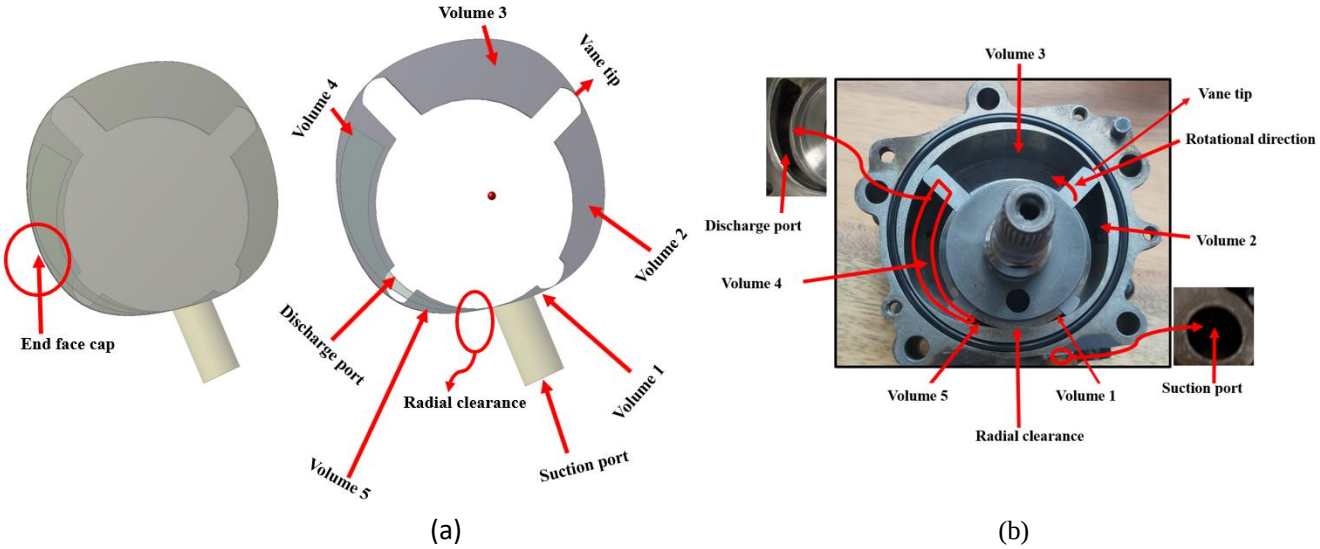

Figure 1(a): Model of the expander prototype; (b): Photograph of the expander prototype

Table 1: Geometries of the expander model

Items	Values	Dimensions
Angle range of inlet port	10° – 100°	-
Angle range of outlet port	225° – 340°	-
Radius of the rotor	27.7	mm
Radius of the stator	38.2-40.7	mm
Suction port diameter	6	mm
Discharge groove width	4-10	mm
Length of the cylinder	38.6	mm
Number of vanes	4	-
Blade thickness	8	mm
Blade tip profile radius	6	mm
Radial clearance gap	0.05	mm
Rotor-vane endface clearance gap	0.1	mm
Vane tip clearance gap	0.1	mm

Table 2: Numerical setup used for the solver

Criteria	Settings	Remarks
Mesh in ports	Hexahedral with boundary layer refinements	Ansys pre-processor
Inlet boundary condition	Pressure inlet	Specified temperature and total pressure
Outlet boundary condition	Pressure outlet	Static pressure with no backflow
Turbulence model	SST – k omega	Standard wall functions with no slip
Transient scheme	First order	Fully implicit Backward Euler
Control volume gradients	Least square cell-based scheme	
Spatial discretization	First order upwind	For stability
Relaxation parameters	Pressure: 0.2 Density: 1 Momentum: 0.7 Turbulent kinetic energy: 0.8 Turbulent dissipation rate: 0.8 Turbulent viscosity: 0.9 Energy: 0.9	For stability
Solver	Pressure based SIMPLE Scheme	
Convergence criterion	1e -03	r.m.s residual level

A hexahedral unstructured mesh containing 758,546 control volumes with inflation layers, with a stretching factor of 1.1- and first-layer height of 0.5 mm, was utilized such that the average y+ value was significantly less than 1 (~0.3), in order to properly model the boundary layers close to the walls. The mesh was generated using the ANSYS ICEM software and is shown in Figure 2. In order to obtain a good mesh quality, orthogonalisation, smoothing and transfinite interpolation were used. The boundary conditions for the simulation such as the inlet and outlet pressures and the inlet temperature were obtained from the experimental conditions used for the validation (Murthy et al., 2022).

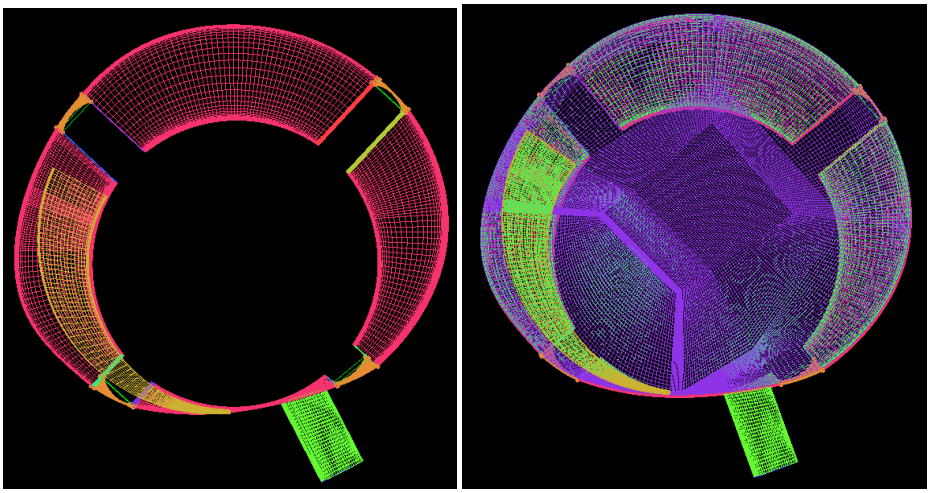

Figure 2: Mesh of the model

2.1 Grid dependency study

A mesh sensitivity study was done using the method of Roche and Celik (Celik et al., 2008) using three different meshes with 411,670, 758,546 and 1,384,556 cells. The simulation results considering the case of 5 bar (g) and 293 K suction conditions with three different meshes namely fine, medium and coarse grids, are summarized in Table 3.

Table 3: Mesh Independent test for CFD Simulation 5 bar (g) at 293.8 K

Test No	Mesh	Nodes	Mass flow rate (kg/h)	CFD Simulation time
1	Coarse (e1)	411670	35.5	24mins
2	Medium (e2)	758546	36.0	40mins
3	Fine (e3)	1384556	36.4	56mins

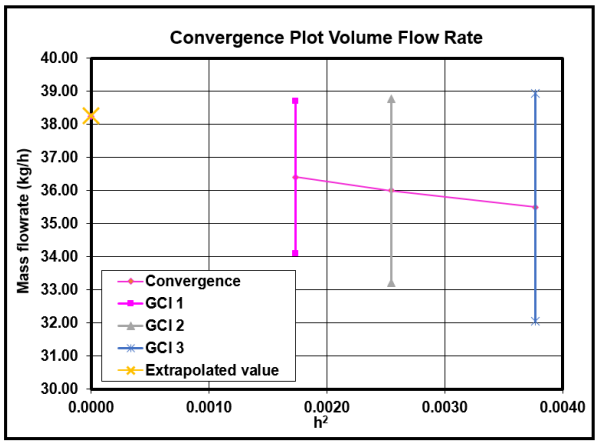

Figure 3: Grid Independence Test for mass flow rate

The effect of grid refinement on the calculated mass flow rate is shown in Figure 3, with the value of the calculated mass flow plotted as a function of nominal mesh size, together with the exact value determined using Richardson extrapolation. The nominal mesh size is represented by *h*, and the error bars show the uncertainty in the solution from the GCI calculation. It was observed that the difference between the coarse and fine grid was less than 3.85%. This level was considered reasonable and could be compared to (Rane et al. 2013) where the change in mass flowrate was less than 6.3% between the two finest grids. The local apparent order *p* was 2.12, demonstrating it was close to second order. This apparent order of the accuracy was used to calculate the (Grid Convergence Index) GCI indices values for coarse, medium, and finer meshes. The relative GCI index values of the mass flow rate for the coarse, medium and fine meshes were found to be 0.06, 0.124 and 0.205, respectively. In order to minimize computation time while maintaining accuracy, the medium mesh was chosen for further analysis.

3. RESULTS AND DISCUSSIONS

3.1 Comparison of CFD predictions of leakage with experimental results

In the present study, the radial clearance, the vane tip, and the rotor-vane endface leakages were investigated at various suction pressures from 0.5 bar (g) to 5 bar (g), constant suction temperature of 25°C and a constant discharge pressure of 0 bar (g), and the results were compared with previously published experimental results (Murthy et al. 2022). Figure 4 (a) shows the comparison between the CFD and experimental mass flow rates of the expander at different suction pressures. The relative error between the CFD mass flow rate and experimental data can be calculated using Equation (1).

$$\text{Relative error} = \left| \frac{\dot{m}_{exp} - \dot{m}_{CFD}}{\dot{m}_{exp}} \right| \quad (1)$$

where $\dot{m}_{CFD}$ is the mass flow rate calculated with CFD and $\dot{m}_{exp}$ is the measured experimental mass flow rate.

Figure 4 (a) shows that there was a reasonable agreement between the experimental and CFD results. The maximum relative difference between the CFD and experimental results was 8.2 kg/h. To further investigate the phenomena and to study the contributions of the different internal leakages, the individual flow rates of the three main leakage paths measured in static conditions (Murthy et al., 2022) were used for comparison with the CFD data. These are plotted in Figure 4 (b), Figure 5(a) and Figure 5(b). Comparing the experimental values in these figures show that the leakage through the radial clearance gap was the most dominant, followed by that through the vane tip gaps and finally that at the rotor-vane endface. However, the CFD values show that the leakage through the vane tip gap was comparable or even slightly higher than that at the radial clearance.

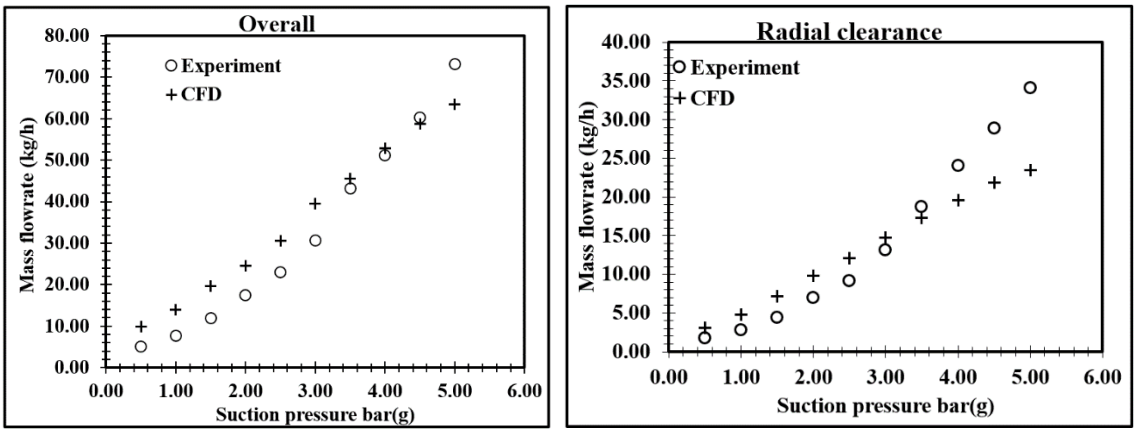

(a) (b)

Figure 4 (a): The simulateds and measured total flow rates; (b) The simulated and measured leakage flow rates through radial clearance

The mass flowrates at the radial clearance obtained from the CFD and the experiments were compared, as shown in Figure 4 (b). They are generally comparable in their values and trends. However, the flowrate measured in the experiments showed an exponential growth with suction pressure. This was because of the change in the gap size as the pressure conditions changed. At lower suction pressures, up to around 2.5 bar (g), there was not enough pressure to change the clearance gap size significantly so the flow rate increased linearly. As the suction pressure increased further from 2.5 to 5 bar (g), the gap size increased and the leakage mass flow rate exhibited exponential growth (Murthy et al., 2022). The increase in suction pressure pushed the rotor in the direction of the resultant force of the pressure difference across the chambers, and this caused the gap width to vary. Meanwhile, the clearances in the CFD model were constant irrespective of suction pressures, so the leakage flow rate through the radial clearance exhibited a linear trend as the suction pressure increased. The average deviations between the experimental and CFD radial clearance gap mass flowrates and overall mass flowrates are 8.2% and 19.7%, respectively.

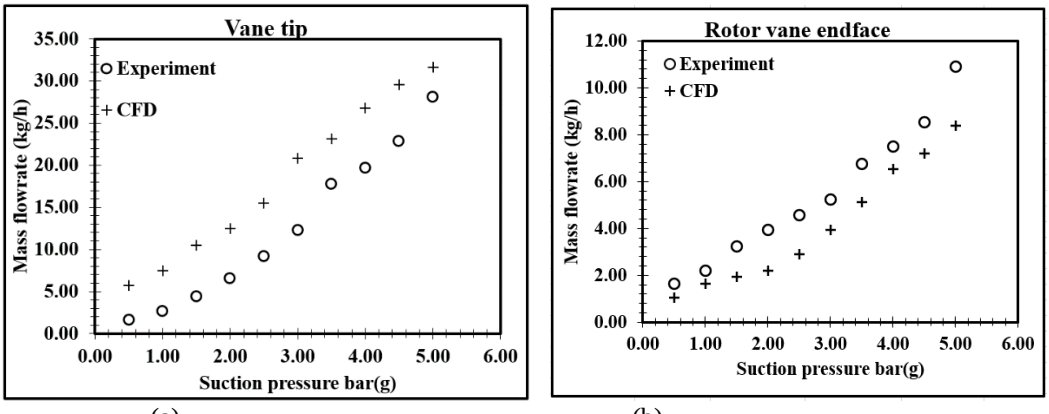

(a) (b)

Figure 5 (a) The simulated and measured leakage flow rates through vane tip gaps; (b) The simulated and measured leakage flow rates through the rotor-vane endface clearances

The leakage flow rates at the vane tips from CFD and measurements are compared in Figure 5 (a). The trends are similar with an offset between the two sets of values. The CFD results consistently over-predicted the vane tip leakage mass flow rates compared to the experimental data. It is thought that this was again due to the interaction between the gap size and pressure in the experiments. Pressure difference between the two ends of the bars that formed the vanes might have moved the bars towards the stator inner wall, reducing the gap at one end while increasing that at the other end. Pressure differences across the difference chambers might deflect the vanes, altering the vane tip clearances further. Meanwhile, the CFD model assumed constant and symmetrical gap sizes at all the vane tips. The average deviation between the experimental and CFD vane tip gap mass flowrates is 38.5%.

Figure 5 (b) shows the simulated and measured leakage flow rates at the rotor-vane endface gaps. The trends are similar but the CFD consistently under-predicted the flow rates. Again, the reason is thought to be due to the change in the actual gap sizes after assembly and during operation. The average deviation between the experimental and CFD rotor-vane endface gap mass flowrates is 38.5%.

3.2 Pressure and velocity contours

The pressure and velocity distributions from the CFD model for a suction pressure of 6 bar (abs.) are presented in Figure 6 to Figure 8. Figure 6 shows the pressure contours on the center plane of the expander. Chamber 1 is at a position where the expansion process has just started while Chamber 2 is close to the end of the expansion process. Chambers 3 and 4 are discharging to the outlet, while Chamber 5 is directly connected to the suction port. The average pressures of Chambers 1 to 5 are 5.6 bar(abs), 4.4 bar(abs), 3.6 bar(abs), 1.2 bar(abs) and 1.3 bar(abs), respectively. Due to internal leakages at the radial clearance, vane tip and vane end face gaps, working fluid leaks to the low-pressure working chamber from the adjacent high-pressure ones.

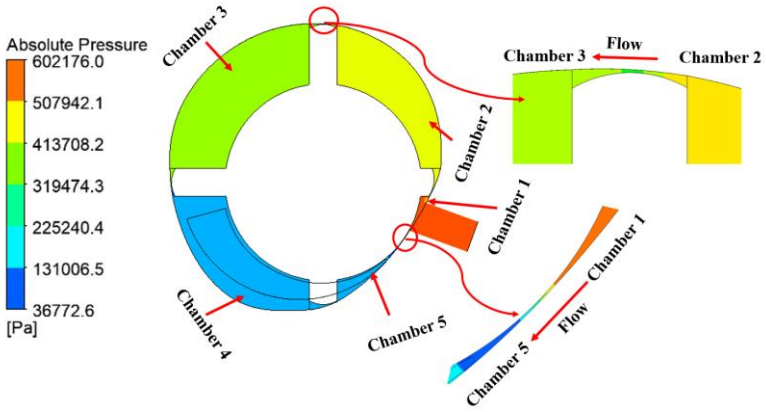

Figure 6: Pressure field at the center of the plane

Figure 7 (a) shows the velocity vectors on the center plane of the expander at the radial clearance. The red color shows the highest value of the velocity and blue the lowest. Due to the converging-diverging geometry and the large pressure ratio of around 5 (upstream pressure of around 5.6 bar, downstream pressure of around 1.3 bar), the flow accelerated until it reached a supersonic speed (as high as 560 m/s) after leaving the throat. This explains the severity of this leakage flow rate as compared to the others discussed in the previous section. Figure 7 (b) shows the magnified view of the leakage flow velocity at the vane tip gap between Chamber 2 (at a pressure of around 4.4 bar) and Chamber 3 (at a pressure of around 3.6 bar). The geometry was again similar to a converging-diverging nozzle, so the fluid was accelerated. However, because the pressure ratio was not too high, the maximum speed was lower than that at the radial clearance.

Contours of the Mach number of the flows on the centre plane at the radial clearance and vane tip gaps are shown in Figure 8. For the radial clearance, shown in Figure 8 (a), the Mach number reached a value of 1.0 at the throat, and then it underwent a supersonic expansion to a maximum value of 2.3 in the downstream direction. This shows the flow was choked at the throat of the clearance and the mass flow rate through the gap was limited by the width of the gap. Figure 8 (b) details the flow regime at the vane tip clearance between Chambers 2 and 3. The Mach number barely reached unity because of the lower pressure ratio.

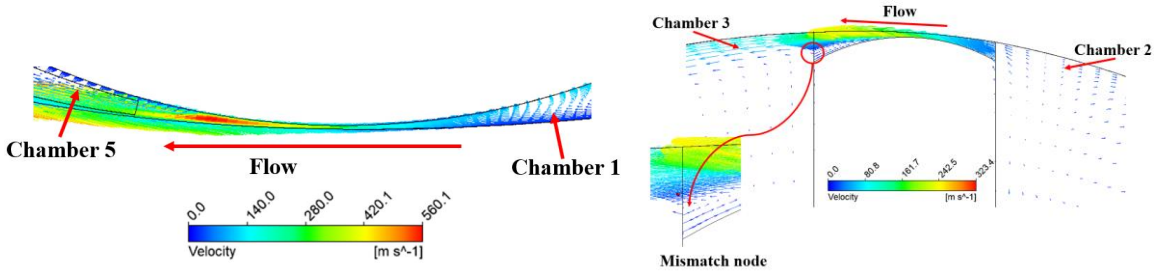

(a) (b)

Figure 7(a): Magnified view of velocity vectors at the radial clearance at suction pressure 5 bar(g); (b) velocity vectors at the vane tip at suction pressure 5 bar(g)

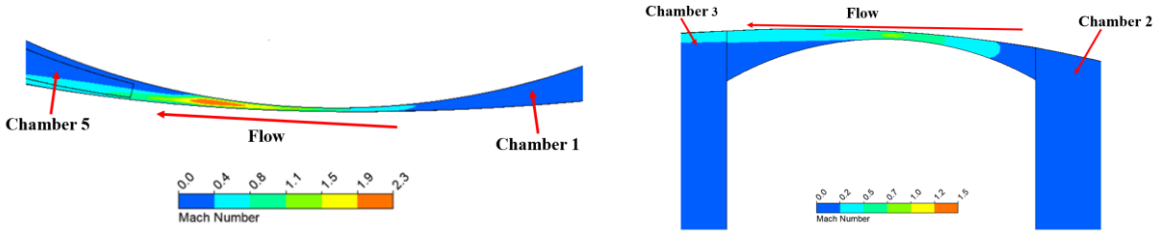

(a) (b)

Figure 8 (a): Mach number distributions at the radial clearance at suction pressure 5 bar(g); (b) Mach number distribution at the vane tip clearance at suction pressure 5 bar(g)

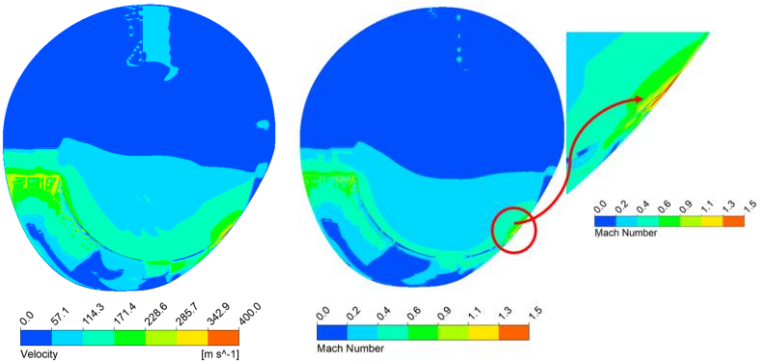

(a) (b)

Figure 9 (a): Magnified view of velocity vectors at the rotor-vane endface at suction pressure 5 bar(g); (b) Mach number distribution at the rotor-vane endface at suction pressure 5 bar(g)

Figure 9 shows the velocity and Mach number at the rotor-vane endface clearance when the suction pressure was 5 bar(g). The contours are plotted in the XY plane, i.e., viewed from the top like the view shown in Figure 1. It can be observed that most of the flows are near the discharge port. The highest velocity was observed at the radial clearance, reaching a Mach number of as high as 1.5, consistent with the results presented above. The leakage at the vane separating chambers 3 and 4 (i.e., the one on the left in Figures 6 and 9) has the second highest velocity, reaching the sound of speed at some places. This was expected considering the pressure ratio between chambers 3 and 4 was around 3.

4. CONCLUSIONS

In this study, a 3D CFD model of the four-intersecting-vane expander has been developed. The mechanism employed two intersecting bars to form the vanes, and a stator that was non-circular. The model was used to obtain the overall flowrate and individual leakage flowrates through the radial clearance, vane tips and rotor end face gaps. The suction pressure was varied from 0.5 bar (g) to 5 bar (g), while the discharge pressure was kept constant at 0 bar (g). Air was used as the working fluid. The experimental and simulated data showed similar trends but some discrepancies were observed in the values. The relative contributions of the leakage paths were found to be somewhat different too. The

experiments showed that the radial clearance was the main contributor compared to the other internal leakage paths (Murthy et al., 2022). However, the CFD analysis suggested that the contributions of the leakage at the vane tip gap was comparable or even slightly more than that at the radial clearance. The main reason behind these discrepancies was thought to be due to the inaccurate gap sizes of the CFD model. These were assumed constant at the values obtained when the expander was disassembled. In reality, the gaps might change during the assembly and the operation. Proper selection of gap sizes is crucial for this study as the flows are often choked, which means the flow rates depended mostly on the gaps and less on the pressures.

In conclusion, the study shows the capability of CFD to study internal leakages of a four-intersecting-vane expander in detail although the accuracy depends on the appropriateness of the assumptions, settings, and boundaries. The results not only provide insights into the flow details, but could provide useful guidance to further improve the design of the machine. In the future, more accurate and realistic simulations can be performed by including the other leakage paths, using dynamic CFD simulation techniques and/or considering the fluid-structure interactions.

ACKNOWLEDGEMENT

The authors thank Dr. Stuart Norris for his advice, support and suggestions for this work.

REFERENCES

ANSYS CFX, URL: www.ansys.com/products/Fluids/ANSYS-CFX

Al-Hawaj, O., 2009. Theoretical modelling of sliding vane compressor with leakage. *Int. J. of Refrig*, *32*(7), 1555-1562. https://doi.org/10.1016/j.ijrefrig.2009.07.005

Badr, O., Probert, S.D., Callaghan, P.O., 1985. Multi-vane expanders: Vane dynamics and friction losses. *Appl. Energy*, *20*(4), 253-285. https://doi.org/10.1016/0306-2619(85)90018-2

Bellmer, F.O., 1966. Rotary vane compressor. U S Patent, 3295752.https://patents.google.com/patent/US3295752

Bianchi, G., Cipollone, R., 2015a. Friction power modeling and measurements in sliding vane rotary compressors. *Appl. Therm. Eng*, *84*, 276-285. https://doi.org/10.1016/j.applthermaleng.2015.01.080

Bianchi, G., Cipollone, R., 2015b. Theoretical modeling and experimental investigations for the improvement of the mechanical efficiency in sliding vane rotary compressors. *Appl. Energy*, *142*, 95-107. https://doi.org/10.1016/j.apenergy.2014.12.055

Bianchi, G., Rane, S., Kovacevic, A., Cipollone, R., 2017. Deforming grid generation for numerical simulations of fluid dynamics in sliding vane rotary machines. *Adv. Eng. Softw*, *112*, 180-191. https://dx.doi.org/10.1016/j.advengsoft.2017.05.010

Cipollone, R., Bianchi, G., Battista, D.D., Contaldi, G., Murgia, S., 2014. Mechanical Energy Recovery from Low Grade Thermal Energy Sources. *Proceedings of the 68th Conference of the Italian Thermal Machines Engineering Association, Energy Procedia*, *45*, 121-130. https://doi.org/10.1016/j.egypro.2014.01.014

Cipollone, R., Bianchi, G., Battista, D., Fatigati, F., 2015. Fuel economy benefits of a new engine cooling pump based on sliding vane technology with variable eccentricity. *Energy Procedia*, *82*, 265-272. https://doi.org/10.1016/j.egypro.2015.12.032

Fukuta, M., Yanagisawa, T., Radermacher, R., 2003. Performance prediction of vane type expander for CO_2 cycle. *The 21st International Congress of Refrigeration at Washington*, 17–22.

Huang, Y.M., Yang, S., 2005. A measurement method for air pressures in compressor vane segments. *Measurement*, *41*(8), 835-841. https://doi.org/10.1016/j.measurement.2005.11.027

Kolasinski, P., Blasiak, P., 2016. Experimental and numerical analyses on the rotary vane expander operating conditions in a micro–Organic Rankine Cycle system. *Energies*, *9*(8), 606. https://doi.org/10.3390/en9080606

Liu, I., Murthy, A.A., Woo, M.W., Subiantoro, A., 2021. Experimental study of the potential use of an expander for atmospheric freeze drying. *Dry. Technol*, https://doi.org/10.1080/07373937.2021.1982963

Murthy, A.A., Subiantoro, A., Norris. S., Fukuta, M., A., 2019. A review on expanders and their performance in vapour compression refrigeration systems. *Int. J. of Refrig*, *106*, 427-446. https://doi.org/10.1016/j.ijrefrig.2019.06.019

Murthy, A.A., Norris, S., Subiantoro, A., 2021a. Experimental analysis of a refurbished heat pump refrigeration system with a four-intersecting-vane expander. *Appl. Therm. Eng*, *183*(1), 116209. https://doi.org/10.1016/j.applthermaleng.2020.116209

Murthy, A.A., Norris, S., Subiantoro, A., 2021b. Effects of lubricating oil on the performance of a Four-Intersecting-Vane Rotary Expander. *IOP conference series Material Science and Engineering*, *1180*, 012030. https://doi.org/10.1088/1757-899X/1180/1/012030

Murthy, A.A., Norris, S., Subiantoro, A., 2022a. Experimental investigation of internal leakages and effects of lubricating oil on the performance of a Four-Intersecting-Vane Rotary Expander. *Energy*, 121689. https://doi.org/10.1016/j.energy.2021.121689

Murthy, A.A., Norris, S., Subiantoro, A., 2022b. Performance of a four-intersecting-vane expander in a R134a refrigeration cycle. *Appl. Therm. Eng*, 118244. https://doi.org/10.1016/j.applthermaleng.2022.118244

Rane, S., Kovacevic, A., Stosic, N., Kethidi, M., 2013. Grid deformation strategies for CFD analysis of screw compressors. *Int. J. of Refrig*, *36*(7), 1883-1893. https://doi.org/10.1016/j.ijrefrig.2013.04.008

Simerics PumpLinx, URL: www.simerics.com/pumplinx

Tang, J.F., Wu, X.D., Wu, Y.Q., Han, G.Q., 2016. Theoretical study of a novel Sliding-Vane Rotary Pump–structure analysis and its chamber pressure. *Part. Sci. Technol*, *35*(2), 247-257. https://doi.org/10.1080/02726351.2016.1211777

Thakur, R., Murthy, A.A., Subiantoro, A., 2019. Investigation of combination of a rotary vane expander and an expansion valve in a refrigeration system. *Proceedings of the 25th IIR International Congress of Refrigeration, Montreal*, *167*, 1-8. http://dx.doi.org/10.18462/iir.icr.2019.0167

Tramschek, A.B., Mkumbwa, M.H., 1996. Mathematical modelling of radial and non-radial rotary sliding vane compressors. *International Compressor Engineering Conference at Purdue University*, 1-9. https://docs.lib.purdue.edu/icec

Vittorini, D., Cipollone, R., 2016. Energy saving potential in existing industrial compressors. *Energy*, *102*, 502-515. https://doi.org/10.1016/j.energy.2016.02.115

Wang, D., Ding, H., Jiang, Y., Xiang, X., 2012. Numerical Modeling of Vane Oil Pump with Variable Displacement. *SAE Tech. Pap*, 2012-01-0637. https://doi.org/10.4271/2012-01-0637

Yang, B., Peng, X., He, Z., Guo, B., Xing, Z., 2009. Experimental investigation on the internal working process of a CO_2 rotary vane expander. *Appl. Therm. Eng*, *29*(11-12), 2289–2296. https://doi.org/10.1016/j.applthermaleng.2008.11.023